Chinese Chemical Letters 32 (2021) 1359–1362

Contents lists available at ScienceDirect

Chinese Chemical Letters

journal homepage: www.elsevier.com/locate/cclet

Communication

Ternary organic solar cells: Improved optical and morphological properties allow an enhanced efficiency

Yingying Zhao[a,1], Liuyang Zhou[b,1], Xiaobo Wu[c], Xiaosha Wang[a], Yungui Li[d], Yazhou Qi[a], Lihui Jiang[a,*], Guohui Chen[a,*], Yingping Zou[a]

[a] College of Chemistry and Chemical Engineering, Central South University, Changsha 410083, China
[b] Beijing National Laboratory for Molecular Sciences, Institute of Chemistry, Chinese Academy of Sciences, Beijing 100190, China
[c] College of Metallurgy and Materials Engineering, Hunan University of Technology, Zhuzhou 412000, China
[d] Max Planck Institute for Polymer Research, Ackermannweg 10, 55128 Mainz, Germany

ARTICLE INFO

Article history:
Received 8 July 2020
Received in revised form 28 August 2020
Accepted 21 September 2020
Available online 22 September 2020

Keywords:
Ternary OSCs
Broaden absorption spectra
Morphology optimization
Appropriate third component

ABSTRACT

The power conversion efficiency (PCE) of OFQx-T:$PC_{71}BM$ blend films reaches 7.59%. On this basis, ternary organic solar cells (OSCs) were fabricated with ITIC or PTB7-Th as the third component. The ternary OSCs with 50 wt% ITIC in acceptors exhibits an enhanced efficiency, from 7.59% to 8.17%. Also, the PCE of ternary OSCs with 50 wt% PTB7-Th in donors achieves 8.72%, which is 13% higher than that of binary OSCs. The PCE improvement of two ternary OSCs is mainly due to the increase of short-circuit current density (J_{sc}), which can be attributed to the complementary absorption spectra and improved film morphology. This work suggests that the selection of an appropriate third component plays a critical role in improving the PCE of ternary OSCs.

Because of various advantages, such as low cost, easy fabrication, large area and flexibility [1–3], organic solar cells (OSCs) have attracted numerous attentions and rapid progress has been achieved after decades of development. The power conversion efficiency (PCE) of single bulk heterojunction (BHJ) has raised to over 18% *via* materials innovation, device engineering and interface processing [4–6]. Nevertheless, relatively narrow absorption spectra of binary OSCs still restricts the value of short-circuit current density (J_{sc}) [7,8]. To make full use of the sunlight, the tandem OSCs have been researched and fabricated [9,10]. Through the complementary absorption of each active layer, tandem OSCs can exhibit a wide absorption spectrum in the visible-near infrared region (vis-NIR) [11–13]. Chen and his colleagues reported tandem OSCs with a record-breaking PCE of 17.3% with the absorption onset of ~1050 nm [9]. Unfortunately, the fabrication of tandem OSCs based on solution processing requires complicated technical processes, giving rise to low productivity and high costs, which might hinder further industrial production of tandem OSCs [14,15]. On the contrary, the active layer of ternary OSCs is composed of two donors and one acceptor, or one donor and two acceptors as a blend to cover the solar spectrum in a broad wavelength range, which makes the fabrication of ternary OSCs easier with a lower cost [16].

It has been demonstrated that a wider absorption spectrum for ternary OSCs is beneficial to reach higher J_{sc} [17]. However, the photovoltaic performance of OSCs is simultaneously determined by J_{sc}, open circuit voltage (V_{oc}) and fill factor (FF), which is related to the absorption spectrum, molecular energy level and morphology of active layers [4,18,19]. The energy levels of three materials in ternary OSCs affect V_{oc} *via* the establishment of cascade energy level structures, which can eventually influence the charge dissociation [20]. In addition, the film morphology can also have a significant impact on charge transport and collection, which is linked to FF for the device [21,22]. Unlike binary OSCs, ternary OSCs generally propose more complex morphology and more recombination centers, therefore, the compatibility of three materials is particularly important for the morphology of active layers [23,24]. Therefore, the careful selection of materials is a prerequisite for high performance ternary OSCs [25,26]. Additionally, to obtain the maximum value of V_{oc}, J_{sc} and FF, device engineering to fine film morphology is essential [27,28]. Until now, research of ternary OSCs has made great progress, and the reported efficiency currently exceeding 17% [20,29].

From our previous work, the PCE of binary OSCs based on OFQx-T:$PC_{71}BM$ is 7.59% [30]. In this work, we selected a medium band

* Corresponding authors.
E-mail addresses: jianglh@csu.edu.cn (L. Jiang), gh-ch@163.com (G. Chen).
[1] These authors contributed equally to this work.

https://doi.org/10.1016/j.cclet.2020.09.032

gap polymer donor PTB7-Th and a medium band gap non-fullerene acceptor ITIC as the third component to prepare ternary OSCs to improve the photovoltaic performance of OFQx-T:$PC_{71}BM$ blends. The optimal PCE of two ternary OSCs reaches 8.17% and 8.72% with ITIC and PTB7-Th as the third component, respectively. The improvement of PCE is mostly ascribed to the enhanced J_{sc}, resulting from the improved photon harvesting, more balanced mobility and weaker bimolecular recombination.

The chemical structures of OFQx-T, PTB7-Th, ITIC, $PC_{71}BM$ are illustrated in Fig. 1. Normalized ultraviolet-visible (UV–vis) absorption spectra of neat OFQx-T, ITIC, PTB7-Th, $PC_{71}BM$ films are shown in Fig. S1 (Supporting information). The normalized absorption spectrum of blend films OFQx-T:$PC_{71}BM$, OFQx-T:$PC_{71}BM$:ITIC and PTB7-Th: OFQx-T:$PC_{71}BM$ are shown in Fig. 2a. The absorption onset (λ_{onset}) of OFQx-T, ITIC, PTB7-Th is 727 nm, 776 nm and 759 nm, respectively. From Fig. 2a, it is apparent that addition of ITIC or PTB7-Th can effectively extend the absorption spectrum of OFQx-T:$PC_{71}BM$ blend films.

The electrochemical properties of four materials were measured by cyclic voltammetry (CV), which are shown in Fig. S2 (Supporting information). The energy level diagrams of four materials can be estimated by the corresponding onsets of oxidation and reduction potentials. Fig. 2b shows the highest occupied molecular orbital (HOMO) and the lowest unoccupied molecular orbital (LUMO) energy levels of these used materials in the active layer. The detailed optical and electrochemical data are listed in Tables S1 and S2 (Supporting information). In OFQx-T:$PC_{71}BM$:ITIC blend films, it is observed that the cascade energy level structures are built during three contents, which provides more charge transfer channels. Similar effects is anticipated for the PTB7-Th:OFQx-T:$PC_{71}BM$ blend films.

The photovoltaic properties of binary and ternary OSCs were investigated with the traditional structure of ITO/PEDOT:PSS/active layer/ZrAcac/Al. And all OSCs were characterized under AM 1.5 G simulated solar light with an intensity of 100 mW/cm^2. The current density-voltage (*J-V*) curves and optimal photovoltaic parameters of binary and ternary OSCs are shown in Fig. 2c and summarized in Table 1, respectively. And photovoltaic parameters of binary and ternary OSCs with different conditions are listed in Table S2. The PCE of binary OFQx-T:$PC_{71}BM$ (1:1.5) blend films is 7.59%, with a V_{oc} of 0.86 V, a J_{sc} of 12.26 mA/cm^2 and FF of 72%. With the simple ternary strategy, the PCE of the as cast OSCs were 4.54% and 4.15% by doping with 50 wt% ITIC or 50 wt% PTB7-Th. As seen in Table S3 (Supporting information), we tried to adjust the proportion of three components, the amount of 1,8-diiodooctane (DIO) and thermal annealing to optimize the photovoltaic characteristics of ternary OSCs. The content of solvent additive DIO has a huge effect on the film forming process of active layers, and finally affects the surface morphology of the blend films. By optimizing the amount of DIO [31], J_{sc} of two ternary OSCs is greatly improved. The OFQx-T:$PC_{71}BM$:ITIC blend films reaches the optimal PCE of 8.17% with a V_{oc} of 0.89 V, J_{sc} of 14.35 mA/cm^2 and FF of 64% by 1% DIO treatment. Similarly, optimal PCE of devices based on PTB7-Th:OFQx-T:$PC_{71}BM$ is 8.72%, with a V_{oc} of 0.82 V, J_{sc} of 14.77 mA/cm^2 and FF of 72% after 1% DIO treatment.

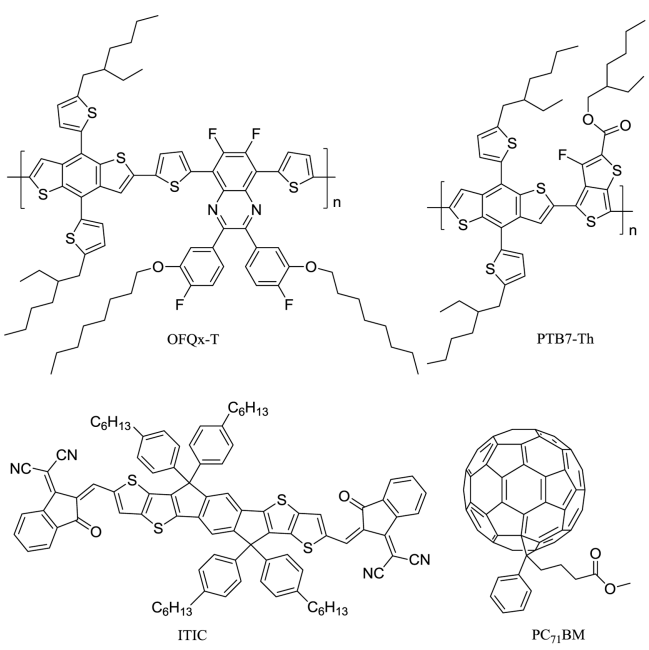

Fig. 1. The chemical structures of OFQx-T, PTB7-Th, ITIC, $PC_{71}BM$.

The external quantum efficiency (EQE) curves of the binary and ternary OSCs are presented in Fig. 2d. Binary OSCs shows a strong response in 300–750 nm, the addition of ITIC and PTB7-Th broadens the photo response spectrum about 50 nm in the NIR region. Compared with binary OSCs, the light absorption intensity of ternary OSCs is greatly enhanced, and maximum EQE value of PTB7-Th:OFQx-T:$PC_{71}BM$ blend films reaches 73%. The calculated J_{sc} of binary OSCs based on OFQx-T:$PC_{71}BM$ of 11.90 mA/cm^2 is enhanced to ternary OSCs of 13.90 mA/cm^2 for OFQx-T:$PC_{71}BM$:ITIC and 14.34 mA/cm^2 for PTB7-Th:OFQx-T:$PC_{71}BM$ respectively. Compared with *J-V* curves, the calculated J_{sc} shows the error less than 3%, proving the reliability of J_{sc}.

In order to investigate the charge recombination in binary and ternary OSCs, we measured the current density (J_{sc}) as a function of light intensity (P_{light}). The relationship of J_{sc} and P_{light} follows the formula of $J_{sc} \propto P_{light}^{\alpha}$, when exponential factor α approaches 1, bimolecular type recombination in devices plays only a minor role for energy losses [32]. As shown in Fig. 3a, the α value of OFQx-T:$PC_{71}BM$ based devices is 0.94. The α of OFQx-T:$PC_{71}BM$:ITIC and PTB7-Th:OFQx-T:$PC_{71}BM$ ternary OSCs are 0.95 and 0.96, respectively. This result demonstrates that two ternary OSCs have a higher α compared to binary devices, indicating weaker bimolecular recombination in ternary devices.

To further explore the charge generation and collection efficiency in devices, we measured the variation curves of the photocurrent density (J_{ph}) with effective voltage (V_{eff}), as shown in Fig. 3b. J_{ph} is described as J_D-J_L, where J_D and J_L is the current densities under standard simulated dark and light conditions, respectively. And V_{eff} is considered to be in V_0 -V_{appl}, in which V_0 is the voltage when $J_D = J_L$, and V_{appl} is the applied voltage in devices. As is known, J_{ph} will achieve a saturation value with the increase of V_{eff}, namely saturation current density (J_{sat}). The J_{ph}/J_{sat} ratio indicates the efficiency of charge dissociation and collection under the maximum power output condition [33]. The J_{ph}/J_{sat} ratio of OFQx-T:$PC_{71}BM$ blend films is 89.58% at $V_{eff} = \sim 0.2$ V. By contrast, J_{ph}/J_{sat} ratio of OFQx-T:$PC_{71}BM$:ITIC and PTB7-Th:OFQx-T:$PC_{71}BM$ blend films are 86.95% and 98.32%, respectively. Exciton dissociation and collection are not ideal in OFQx-T:$PC_{71}BM$:ITIC blend films, which reduces the FF. The devices based on PTB7-Th:OFQx-T:$PC_{71}BM$ exhibit a higher exciton dissociation and collection efficiency, resulting in higher J_{sc}.

The hole and electron mobility of binary and ternary OSCs were investigated through space-charge limited current (SCLC) method based on single carrier devices [34]. The device structure of the hole-only and electron-only is ITO/PEDOT:PSS/active layer/Au and ITO/ZnO/active layer/PDINO/Al, respectively. Figs. 3c and d show the $J^{1/2}$-*V* curves of binary and ternary OSCs. And detailed data for electron mobility (μ_e) and hole mobility (μ_h) are provided in Table S4 (Supporting information). The μ_e and μ_h of binary OSCs are 1.69×10^{-4} cm^2 V^{-1} s^{-1} and 1.09×10^{-4} cm^2 V^{-1} s^{-1}, with the mobility ratio μ_e/μ_h of 1.55. The OFQx-T:$PC_{71}BM$:ITIC blend films

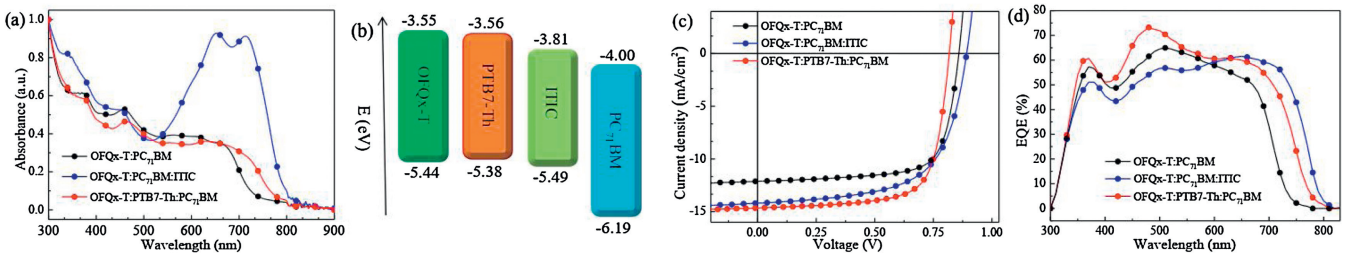

Fig. 2. (a) Absorption spectrum of OFQx-T:$PC_{71}BM$, OFQx-T:$PC_{71}BM$:ITIC and PTB7-Th:OFQx-T:$PC_{71}BM$ blend films in thin film; (b) Energy level diagrams of OFQx-T, PTB7-Th, ITIC, $PC_{71}BM$; (c) *J-V* characteristics of binary and ternary OSCs under illumination of AM 1.5 G at 100 mW/cm^2; (d) EQE curves of binary and ternary OSCs.

Table 1
Photovoltaic parameters of binary and ternary OSCs with optimal conditions.

Active layer[a]	Ratio	V_{oc} (V)	J_{sc} (mA/cm^2)	FF (%)	PCE (max%)
OFQx-T:$PC_{71}BM$[b]	1:1.5	0.86	12.26	72	7.59
OFQx-T:$PC_{71}BM$:ITIC[b]	1:0.75:0.75	0.89	14.35	64	8.17
OFQx-T:PTB7-Th:$PC_{71}BM$[b]	0.5:0.5:1.5	0.82	14.77	72	8.72

[a] The total concentration is 20 mg/mL.
[b] With 1% DIO as solvent additive.

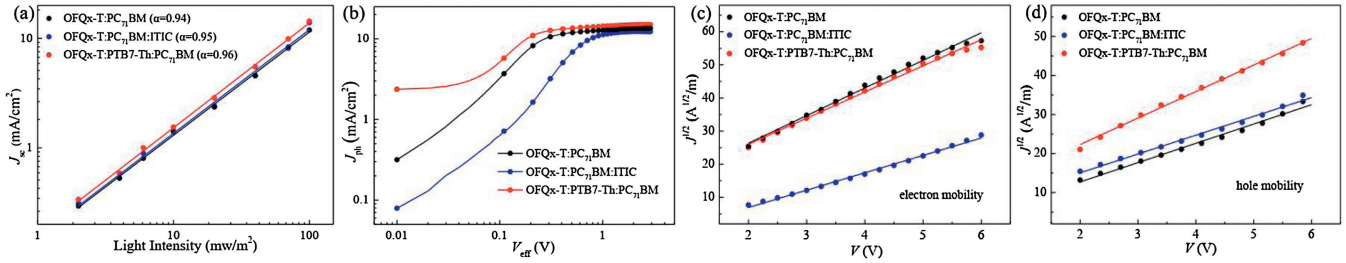

Fig. 3. (a) Light intensity dependence of J_{sc} of the binary and ternary OSCs; (b) J_{ph} -V_{eff} characteristics of the binary and ternary OSCs; (c) The electron mobilities of binary and ternary OSCs; (d) The hole mobilities of binary and ternary OSCs.

show the μ_e of 1.59×10^{-4} cm^2 V^{-1} s^{-1}, μ_h of 1.34×10^{-4} cm^2 V^{-1} s^{-1} with μ_e/μ_h of 1.19. And PTB7-Th:OFQx-T:$PC_{71}BM$ blend films exhibit the μ_e of 2.78×10^{-4} cm^2 V^{-1} s^{-1}, μ_h of 2.06×10^{-4} cm^2 V^{-1} s^{-1} with μ_e/μ_h of 1.35. The ternary OSCs have a more balanced mobility, which is beneficial for higher J_{sc} [35]. Moreover, higher and more balanced mobility facilitates higher J_{sc} for PTB7-Th-based ternary OSCs.

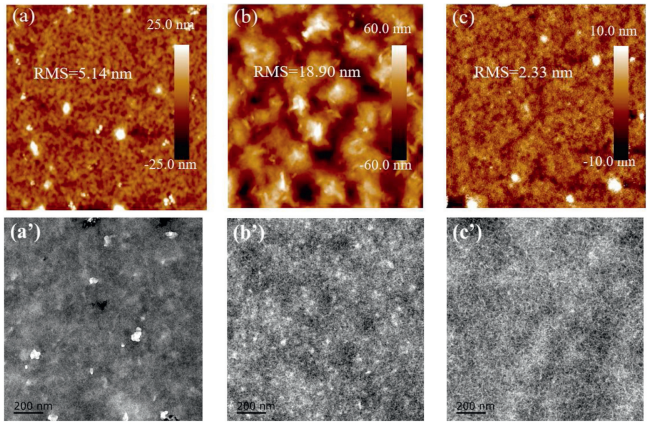

Fig. 4. (a-c) AFM images (5×5 μm^2) and (a'-c') TEM images of binary and ternary OSCs. (a, a') OFQx-T:$PC_{71}BM$ blend films; (b, b') OFQx-T:$PC_{71}BM$:ITIC blend films; (c, c') PTB7-Th:OFQx-T:$PC_{71}BM$ blend films.

We further considered the blends morphology of binary and ternary OSCs through atomic force microscopy (AFM) and transmission electron microscopy (TEM). The AFM and TEM images are shown in Fig. 4. The root-mean-square (RMS) of OFQx-T:$PC_{71}BM$ blend films is 5.14 nm. The RMS values of ternary OSCs with ITIC and PTB7-Th are 18.90 nm and 2.33 nm, respectively. It indicates that for OFQx-T:$PC_{71}BM$ blend films, PTB7-Th with a smaller value has better compatibility. The effect of ITIC and PTB7-Th on blends morphology can be observed from TEM images, and the bright and dark zones are donor-rich and acceptor-rich domain, respectively [36]. Fig. 4a' shows a good blending between OFQx-T and $PC_{71}BM$, resulting in OFQx-T:$PC_{71}BM$ minor phase separation. Although small separation size is conducive to excitons dissociation, it also limits the carrier transport to a certain extent. As seen, two ternary OSCs blend films exhibit a proper phase separation, especially a clear network structure was observed in PTB7-Th:OFQx-T:$PC_{71}BM$ blends. It suggests that smooth surface morphology and nanoscale network interpenetrating structure are beneficial to efficient exciton dissociation and charge transport. This work also illustrates the importance of a suitable third content to device morphology.

In conclusion, ternary OSCs with ITIC or PTB7-Th as the third component have been fabricated successfully. Compared with the binary OSCs based on OFQx-T:$PC_{71}BM$ blends with efficiency of 7.59%, PCE of ternary OSCs increases to 8.17% with 50 wt% ITIC as a complementary acceptor. Meanwhile, efficiency of the optimized ternary OSCs with 50 wt% PTB7-Th into donors can be enhanced to 8.72% with a relative of 13% improvement. The additional

absorption of the third component in ternary OSCs can enhance light harvesting and J_{sc}. The third component can also give rise to a more balance charge carrier mobility and weaker bimolecular recombination, which can also contribute to higher J_{sc}. Moreover, the PTB7-Th:OFQx-T:$PC_{71}BM$ blend films shows a clear network interpenetrating structure, giving rise to higher exciton dissociation and collection efficiency. This work suggests that ternary OSCs with an appropriate third component can be useful to improve device performance of binary donor-acceptor OSCs.

Declaration of competing interest

The authors report no declarations of interest.

Acknowledgments

This study has been supported by the National Natural Science Foundation of China (No. 21506258) and Natural Science Foundation of Hunan Province (Nos. 2016JJ3134, 2017JJ2325).

Appendix A. Supplementary data

Supplementary material related to this article can be found, in the online version, at doi:https://doi.org/10.1016/j.cclet.2020.09.032.

References

[1] Q. Wei, W. Liu, M. Leclerc, et al., Sci. China Chem. 63 (2020) 1352–1366.
[2] L. Lu, T. Zheng, Q. Wu, et al., Chem. Rev. 115 (2015) 12666–12731.
[3] J. Yuan, Y. Zhang, L. Zhou, et al., Joule 3 (2019) 1140–1151.
[4] G. Zhang, J. Zhao, P.C.Y. Chow, et al., Chem. Rev. 118 (2018) 3447–3507.
[5] X. Xu, Z. Bi, W. Ma, et al., Adv. Mater. 29 (2017) 1704271.
[6] Q. Liu, J. Qin, J. Xu, et al., Sci. Bull. 65 (2020) 272–275.
[7] W. Huang, P. Cheng, Y.M. Yang, et al., Adv. Mater. 30 (2018) 1705706.
[8] W. Zhao, S. Li, H. Yao, et al., J. Am. Chem. Soc. 139 (2017) 7148–7151.
[9] L. Meng, Y. Zhang, X. Wan, et al., Science 361 (2018) 1094–1098.
[10] Y. Cui, B. Gao, Y. Qin, et al., J. Am. Chem. Soc. 139 (2017) 7302–7309.
[11] T.Y. Li, T. Meyer, Z. Ma, et al., J. Am. Chem. Soc. 139 (2017) 13636–13639.
[12] K. Zhang, K. Gao, R. Xia, et al., Adv. Mater. 28 (2016) 4817–4823.
[13] X. Lia, K. Li, S. Dan, et al., Chin. Chem. Lett. 31 (2020) 1243–1247.
[14] P. Cheng, C. Yan, Y. Wu, et al., Adv. Mater. 28 (2016) 8021–8028.
[15] Q. An, F. Zhang, J. Zhang, et al., Energy Environ. Sci. 9 (2016) 281–322.
[16] H. Huang, B. Sharma, J. Mater. Chem. A 5 (2017) 11501.
[17] X. Ma, M. Luo, W. Gao, et al., J. Mater. Chem. A 7 (2019) 7843–7851.
[18] M. Luo, C. Zhu, J. Yuan, et al., Chin. Chem. Lett. 30 (2019) 2343–2346.
[19] A. Wadsworth, M. Moser, A. Marks, et al., Chem. Soc. Rev. 48 (2019) 1596–1625.
[20] L. Zhan, S. Li, T.K. Lau, et al., Energy Environ. Sci. 13 (2020) 635–645.
[21] R. Yu, H. Yao, Y. Cui, et al., Adv. Mater. 31 (2019) 1902302.
[22] W. Gao, C. Zhong, G. Zhang, et al., ACS Energy Lett. 3 (2018) 1760–1768.
[23] Y. Xie, F. Yang, Y. Li, et al., Adv. Mater. 30 (2018) 1803045.
[24] K. Weng, P. Bi, H. Ryu, et al., J. Mater. Chem. A 7 (2019) 3552.
[25] X. Ma, Y. Mi, F. Zhang, et al., Adv. Energy Mater. 8 (2018) 1702854.
[26] H. Hu, L. Ye, M. Ghasemi, et al., Adv. Mater. 31 (2019) 1808279.
[27] J. Wang, W. Gao, Q. An, et al., J. Mater. Chem. A 6 (2018) 11751–11758.
[28] Y. Cho, S. Jeong, S. Lee, et al., Nano Energy 75 (2020) 104896.
[29] X. Du, L. Zhou, H. Lin, et al., Adv. Funct. Mater. 30 (2020) 1909837.
[30] S. Xu, L. Feng, J. Yuan, et al., Org. Electron. 50 (2017) 7–15.
[31] S. Xie, J. Wang, R. Wang, et al., Chin. Chem. Lett. 30 (2019) 217–221.
[32] M. Zhang, F. Zhang, Q. An, et al., Nano Energy 22 (2016) 241–254.
[33] L. Huo, T. Liu, X. Sun, et al., Adv. Mater. 27 (2015) 2938–2944.
[34] D.F. Barbe, J. Phys. D: Appl. Phys. 4 (1971) 1812.
[35] S.S.M. Stolterfoht, A. Armin, H. Jin, et al., Adv. Mater. 7 (2017) 1601379.
[36] Y. Zhong, M.T. Trinh, R. Chen, et al., Nat. Commun. 6 (2015) 8242.